Green Chemistry

PAPER

View Article Online
View Journal | View Issue

Cite this: *Green Chem.*, 2025, **27**, 3573

Integrated biorefinery routes to transform furfural waste into 2G biofuels and PFOA-adsorbing biochar†

Yuting Tan,[a] Meysam Madadi, *[a] Guojie Song,[a] Chihe Sun,[a] Mahdy Elsayed,[b] Fubao Sun*[a] and Vijai Kumar Gupta[c]

Received 14th January 2025,
Accepted 3rd March 2025

DOI: 10.1039/d5gc00199d

rsc.li/greenchem

This study presents a cutting-edge decentralized biorefinery approach that valorizes furfural residues (FRs) into high-value products, including ethanol, bio-oil (emphasizing bio-phenols), and perfluorooctanoic acid (PFOA)-adsorbing biochar. Employing an advanced acid/glycerol pretreatment with fatty alcohol polyoxyethylene ether (AEO), surfactant significantly enhances FR fractionation of FRs. The AEO plays a crucial role in pretreatment by weakening cellulose-lignin interactions, enhancing pore characteristics, and preventing pseudo-lignin formation in FRs. These modifications increase cellulose hydrolysis efficiency, facilitating the conversion of cellulose-rich residues into 198 g kg^{-1} ethanol through hydrolysis and fermentation. The remaining lignin undergoes pyrolysis, producing 184 g kg^{-1} bio-oil, with a phenol content of 77.5% and 237 g kg^{-1} biochar. The biochar's potential for adsorbing PFOA is evaluated, costing just 1.5–1.8 cents per gram, offering a sustainable method for environmental remediation. Detailed physicochemical and computational analyses reveal that PFOA adsorption on biochar surfaces involves electrostatic interactions, hydrogen bonding, and hydrophobic interactions. The study further evaluates this approach's economic and environmental viability, highlighting a minimum biochar selling price of US $ 41.81 per ton FRs and CO_2 emissions of 936 g CO_2 per kg biochar. This research reaffirms the potential of FRs as a sustainable feedstock for biofuel and bioproduct production, advancing circular bioeconomy principles.

Green foundation

1. This work advances green chemistry by developing a sustainable method to valorize furfural residues into biofuels and biochar, integrating waste utilization, pollution mitigation, and resource recovery. The process enhances cellulose hydrolysis, produces biofuels, and generates biochar for PFOA adsorption, supporting the circular bioeconomy.
2. We developed a cost-effective biorefinery process that produces biochar with remarkable PFOA adsorption (1.5–1.8 cents per gram). Additionally, the biochar has a minimum selling price of US$ 41.81 per ton and low CO_2 emissions of 936 g CO_2 per kg biochar, ensuring both economic and environmental feasibility.
3. Future research should focus on refining process efficiencies and integrating renewable energy systems, which would reduce environmental impact and enhance the scalability and economic feasibility of the biorefinery for broader industrial adoption.

1. Introduction

The global population's unprecedented growth and rapid economic expansion have exacerbated the challenges posed by climate change. This situation is further intensified by an increasing dependence on fossil fuels, underscoring an urgent imperative for sustainable energy solutions.[1] In this context, lignocellulosic biomass (LCB), the most abundant plant-based resource available, emerges as a promising avenue toward achieving carbon neutrality. As a low-cost, non-food feedstock,

[a]*Key Laboratory of Industrial Biotechnology, Ministry of Education, School of Biotechnology, Jiangnan University, Wuxi 214122, China.*
E-mail: m.madadi@jiangnan.edu.cn, fubaosun@jiangnan.edu.cn
[b]*Department of Agricultural Engineering, Faculty of Agriculture, Cairo University, Giza 12613, Egypt*
[c]*School of Biotechnology, Dublin City University, Glasnevin, Dublin, D09 K20V, Ireland*

† Electronic supplementary information (ESI) available. See DOI: https://doi.org/10.1039/d5gc00199d

LCB holds substantial potential for producing biofuels and platform chemicals, facilitating the development of more sustainable energy systems.[2]

Among the various chemicals derived from LCB, furan-based compounds, particularly hydroxymethylfurfural and furfural (FF), are of significant interest. FF has been identified as one of the twelve essential platform chemicals produced in LCB biorefineries, playing a critical role in the synthesis of jet fuels, polymers, pharmaceuticals, and agrochemicals.[3] With annual production exceeding 300 ktons and a growth rate of approximately 2%, FF is primarily obtained through the acid hydrolysis of pentose-rich LCB sources.[4] However, this process, which employs high temperatures and mineral or heterogeneous acids, generates substantial quantities of furfural residues (FRs), with an annual production of 772 ktons, rich in cellulose and lignin.[3] Unfortunately, current disposal methods for these residues, including composting and incineration, pose significant environmental challenges, such as pollution, nutrient depletion, and increased greenhouse gas emissions. To mitigate these impacts, innovative biorefinery strategies are essential for converting FRs into valuable products, thus reducing their environmental footprint and supporting the transition to sustainable energy systems.

The effective conversion of FRs into valuable products hinges on selecting appropriate biorefining techniques. Given their rich cellulose and lignin content, FRs present considerable opportunities for the production of ethanol and bio-oil. However, the complex interactions between cellulose and lignin significantly hinder further processing.[54] Addressing these challenges necessitates a robust pretreatment strategy to disrupt these interactions.[6] The conventional pretreatment method for FRs typically involves strong oxidizing agent alkaline pretreatment underhigh temperatures for improving lignin removal efficiency towards enhanced enzymatic hydrolysis. However, this process often uses a high dose of catalyst and requires high-intensity pretreatment conditions, along with greater cellulosic-sugar loss. Glycerol-based organic solvent pretreatment is considered one of the most promising methods because it can effectively break down the dense structure of biomass, thereby enhancing enzymatic hydrolysis efficiency.[7] Acid-catalyzed glycerol pretreatment requires a lower pretreatment temperature to disrupt the lignin-carbohydrate linkages for achieving significant enzymatic hydrolysis enhancement compared to that of alkali-catalyzed pretreatment.[7] More importantly, the acidic conditions are more favorable for the modification of lignin by glycerol and surfactants.[8,9] Additionally, the effective recovery of glycerol after pretreatment highlights the sustainability of this method.[10]

In FR lignin, one of the most promising applications lies in bio-oil production *via* pyrolysis. This mature technology is recognized for its potential to mitigate CO_2 emissions, aligning well with circular economy principles.[11] During pyrolysis, dried biomass is subjected to high temperatures (400–800 °C) in an inert reactor environment, resulting in the decomposition of biomass into bio-oil, gas, and biochar. High-value chemicals can be extracted from bio-oil and upgraded to produce drop-in liquid biofuels.[12] Our previous investigations indicate that the maximum bio-oil yield from the pyrolysis of FR lignin ranges from 27.9% to 28.3%.[13] However, this relatively low yield is attributed to the inherent unreactivity of FR's lignin, highlighting the need for effective methods to enhance lignin quality and reactivity before the pyrolysis process.

To address the challenges of cellulose hydrolysis and the low yield of bio-oil, adding surfactants like Polysorbate (Tween), Polyethylene Glycol (PEG), and the Triton X series during pretreatment has been found to improve the effectiveness of LCB fractionation and subsequent cellulose hydrolysis. For instance, the addition of Tween 80, PEG 4000, and Triton X-100 in NaOH-catalyzed glycerol pretreatment improved enzymatic hydrolysis of pretreated substrates by 15.7%–38.3%, leading to a 6.4–22.3% increase in ethanol titers.[14] This improvement is due to the dual role of surfactants: they modify the structural properties of the substrate and reduce non-productive interactions between lignin and enzymes. Additionally, surfactants facilitate their grafting into lignin through etherification, which decreases phenolic hydroxyl groups and increases β-O-4 linkages.[15] Thus, it is proposed that implementing surfactants in FRs pretreatment augments ethanol yields and generates reactive lignin conducive to higher bio-oil production.

Furthermore, the biochar produced from residual lignin after pyrolysis possesses significant potential as an adsorbent for environmental contaminants, such as perfluorooctanoic acid (PFOA).[16,51,52] This persistent organic pollutant is known for its harmful effects on human health and the environment. It is linked to various health issues, including liver damage, developmental disorders, and immune system disruption. The ability of biochar to adsorb PFOA positions it as a valuable tool for mitigating its impact, providing a sustainable solution in the ongoing battle against pollution.[17]

In light of the above, this study introduces a pioneering biorefinery approach for the valorization of FRs, transforming them into biofuels and biochar, thereby addressing critical environmental issues associated with their disposal. The research delineates an advanced acidic glycerol pretreatment integrating surfactants (*e.g.*, Tween 80, PEG 4000, Triton X-100, and Fatty alcohol polyoxyethylene ether (AEO)) to enhance FRs fractionation. Specifically, (i) cellulose-rich residues are converted into ethanol through high-solid enzymatic hydrolysis and yeast fermentation, achieving significant enhancements in ethanol titers attributable to the surfactants' role in optimizing substrate accessibility; (ii) the modified residual lignin resultant from enzymatic hydrolysis is subjected to pyrolysis, yielding high quantities of bio-oil and biochar, alongside minimal gaseous byproducts. Moreover, comprehensive investigations were conducted into the physicochemical transformations of FRs pre- and post-treatment, alongside a detailed analysis of the distribution of key components within the bio-oil. The biochar produced was further evaluated for its efficacy in adsorbing PFOA, with an in-depth exploration of the biosorbent's physicochemical properties and the underlying

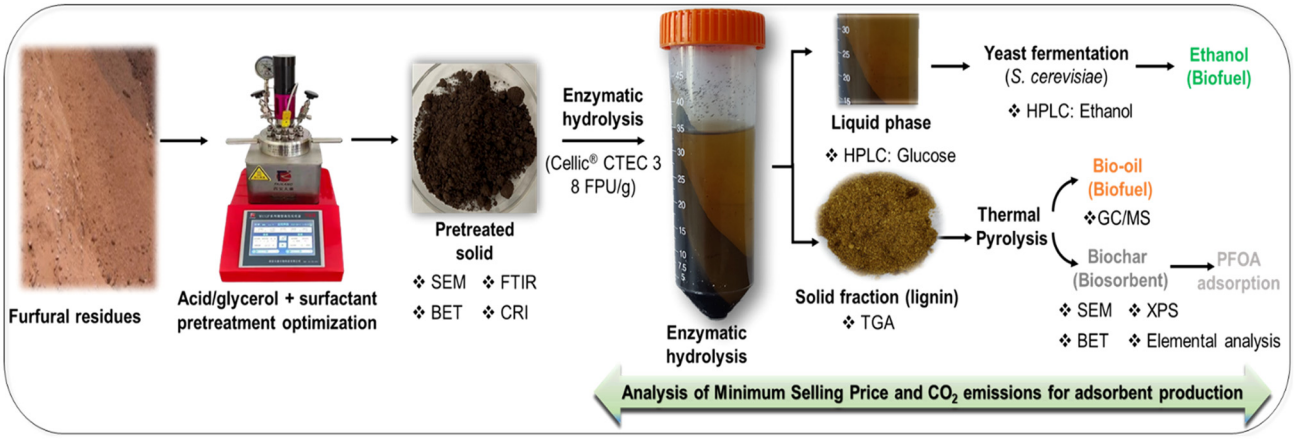

Fig. 1 Flowchart of surfactant-assisted acid/glycerol pretreatment for converting FRs into biofuels (ethanol and bio-oil) with integrated use of biochar for PFOA adsorption. Main analyses included.

adsorption mechanisms. Finally, the potential of the biorefinery process to reduce CO_2 emissions was assessed, alongside an evaluation of its minimum selling price (MSP), underscoring this innovative approach's economic feasibility and environmental sustainability (Fig. 1).

2. Materials and methods

2.1. Materials and reagents

FRs were generously provided by Xin Ji Ju Run Biotechnology Co. Ltd, Hebei, China. The initial pH of the FRs ranged from 2 to 3. The FRs were immersed in water for 24 h, followed by multiple washings until achieving a neutral pH. Subsequently, they were dried at 50 °C for 12 h and then sieved through a 60-mesh sieve. Cellic® CTec 3, exhibiting an activity of 210 FPU g^{-1} (118 mg protein per mL), was sourced from Novozymes Investment Co. Ltd, Beijing, China. The *Saccharomyces cerevisiae* Angel strain was also obtained from Angel Yeast Co. Ltd. Industrial sulfuric acid and glycerol (>95% purity) from Wuxi Chemical Factory, Jiangsu Province, China. All other chemicals were obtained from Sinopharm Chemical Reagent Factory Ltd, China.

2.2. Acid/glycerol pretreatment in the presence of surfactant

The acid/glycerol pretreatment was executed in a temperature- and time-controlled reactor (TK-PCGF-2-250, Xi'an, China) utilizing stainless steel containers, following an established protocol.[13] In this procedure, 10 g of dried FRs were combined with 140 g of a 70% (w/w) glycerol solution, to which 1% (w/w) sulfuric acid was added, along with 5% (w/v) of surfactants (Tween 80, PEG 4000, Triton X-100, and AEO). The resulting mixture was incubated at temperatures ranging from 100 °C to 160 °C for 20 min while maintaining a stirring speed of 300 rpm, based on our previous study.[9] After pretreatment and subsequent cooling, the solid FRs were collected *via* a G1 filter and washed thrice with 100 mL of tap water. The washed FRs were then dried in an oven at 50 °C for 12 h. These pretreated FRs were retained for further analyses, including primary composition analysis, physicochemical characterization, and enzymatic hydrolysis. The cellulose and lignin content in raw and pretreated FRs were analyzed through the National Renewable Energy Laboratory (NREL) protocol.[18] Solid and cellulose recovery rates, as well as lignin removal, were calculated according to eqn (1)–(3);

$$\text{Solid recovery}\,(\%) = \frac{S_2\,(g)}{S_1\,(g)} \times 100 \quad (1)$$

$$\text{Cellulose recovery}\,(\%) = \frac{C_2\,(g)}{C_1\,(g)} \times 100 \quad (2)$$

$$\text{Lignin removal}\,(\%) = 1 - \frac{L_2\,(g)}{L_1\,(g)} \times 100 \quad (3)$$

S_2, C_2, and L_2 represent the mass of pretreated FRs, cellulose, and lignin mass in the pretreated FRs, respectively. Conversely, S_1, C_1, and L_1 denote the mass of raw FRs and the amounts of cellulose and lignin in the raw FRs.

2.3. Separate cellulose hydrolysis and fermentation process

The enzymatic hydrolysis of pretreated FRs was conducted in 100 mL Erlenmeyer flasks. Dried pretreated FRs at a solid loading of 2% (w/v) were combined with 25 mL of citrate buffer (pH 4.8) containing 8 FPU g^{-1} of Cellic® CTec 3 and incubated at 50 °C for 48 h. For high-solid enzymatic hydrolysis, 250 mL Erlenmeyer flasks were used, with pretreated FRs at a loading of 20% (w/v) mixed with 45 mL of citrate buffer (8 FPU g^{-1} CTec 3) and incubated at 50 °C for 72 h. Following previous work, a fed-batch strategy was implemented to mitigate mass transfer resistance.[19] The initial solid loading was set at 8%, with an additional 4% of pretreated FRs added at 6 h, 12 h, and 24 h, ultimately achieving a final solid loading of 20%. At designated time points, 0.4 mL samples were collected, heated at 100 °C for 5 min to inactivate the enzymes, and centrifuged at 10 000 rpm for 5 min. The resulting super-

natant was diluted to an appropriate concentration for glucose analysis.

Ethanol production was performed using the separate hydrolysis and fermentation (SHF) technology. The fermentation occurred in 250 mL flasks containing glucose, engineered *S. cerevisiae* Angel strain, 10 g L^{-1} yeast extract, and 20 g L^{-1} peptone. The fermentation broth was inoculated with 10% yeast and incubated at 37 °C with shaking at 180 rpm for 72 h.

The concentrations of glucose (post-hydrolysis) and ethanol (post-fermentation) were determined using high-performance liquid chromatography (HPLC, Chomaster CM5110, Hitachi, Japan) with a Bio-Rad Aminex HPX-87H packed column (9 μm, 7.8 × 300 mm). The mobile phase consisted of 5 mM dilute sulfuric acid, with an isocratic flow rate of 0.6 mL min^{-1}, and the column temperature was maintained at 60 °C. The yields of glucose and ethanol were calculated according to eqn (4) and (5);

$$\text{Glucose yield}\,(\%) = \frac{\text{Glucose after cellulose hydrolysis}\,(\text{g}) \times 0.9}{\text{Cellulose level in pretreated FRs}\,(\text{g})} \times 100 \quad (4)$$

$$\text{Ethanol yield}\,(\%) = \frac{\text{Ethanol after fermentation}\,(\text{g})}{\text{Glucose}\,(\text{g}) \times 0.51} \times 100 \quad (5)$$

2.4. PFOA adsorption experiments

Biochar samples were used as adsorbents to study PFOA's adsorption kinetics and isotherms. The adsorption equilibrium amount (Q_t) was calculated based on eqn (6):[20]

$$Q_t = \frac{(C_0 - C_t)V}{m} \quad (6)$$

where C_0 and C_t (μg L^{-1}) are the concentrations of PFOA at the initial time and the equilibrium time, respectively. m (g) is the amount of biochar used in the solution, and V (L) represents the volume of the solution.

For the adsorption kinetics experiments, the initial PFOA concentration was maintained at 3.5×10^4 μg L^{-1} in all cases, with the pH adjusted to 7.0 ± 0.2 using 0.1 M HCl and 0.1 M NaOH. A biochar concentration of 1.0 g L^{-1} was introduced, and the system was agitated at 150 rpm, with adsorption measurements taken at intervals of 0, 10, 30, 60, 120, 360, 720, 1440, 2160, and 2880 min to determine the PFOA concentration in the solution. The pseudo-first-order model and pseudo-second-order model were used to fit the adsorption kinetics based on eqn (7) and (8):[21]

$$Q_t = Q_e\,(1 - e^{-K_1 t}) \quad (7)$$

$$\frac{t}{Q_t} = \frac{1}{K_2 Q_e^2} + \frac{t}{Q_e} \quad (8)$$

where Q_e and Q_t are the amounts of PFOA adsorbed onto the adsorbent (μg g^{-1}) at equilibrium and at time t (min), respectively; K_1 (h^{-1}) and K_2 (g μg^{-1} h^{-1}) are the rate constant of the pseudo-first-order model and the pseudo-second-order model.

For the adsorption isotherm studies, initial PFOA concentrations were set at 5×10^3, 10^4, 2×10^4, 5×10^4, 10^5, 1.5×10^5, 2×10^5, and 3×10^5 μg L^{-1}, with pH adjusted to 7.0 ± 0.2 using 0.1 M HCl and 0.1 M NaOH. A biochar concentration of 1.0 g L^{-1} was added, and the mixture was agitated at 150 rpm for 48 h. The Langmuir model, the Freundlich model, the Dubinin–Radushkevich model, and the Sips model were used to fit the adsorption isotherm based on eqn (9)–(12):[21]

$$Q_e = \frac{K_L Q_m C_e}{1 + K_L C_e} \quad (9)$$

$$Q_e = K_f C_e^{1/n} \quad (10)$$

$$Q_e = Q_s e^{(-K_{dr}\varepsilon^2)} \quad (11)$$

$$\varepsilon = RT\,\text{In}\left(1 + \frac{1}{C_e}\right)$$

$$E = \frac{1}{\sqrt{2K_{dr}}}$$

$$Q_e = \frac{Q_{ms} K_s C_e^{\beta}}{1 + K_s C_e^{\beta}} \quad (12)$$

where C_e is the equilibrium concentration (μg L^{-1}) of PFOA in an aqueous solution; Q_e is the equilibrium amount (μg g^{-1}); K_L (L μg^{-1}) and K_f ($\mu g^{1-1/n}$ g^{-1} $L^{1/n}$) are the Langmuir and Freundlich sorption constant, respectively; $1/n$ represents the degree of non-homogeneity of adsorption; $Q_m/Q_s/Q_{ms}$ indicate the maximum sorption capacity (μg g^{-1}); K_{dr} (mol^2 J^{-2}) presents the activity coefficient related to sorption mean free energy; ε denotes the Dubinin–Radushkevich isotherm constant; R and T are the ideal gas constant (8.314 kJ mol^{-1} K^{-1}) and the temperature in terms of Kelvin (K), respectively; the E (kJ mol^{-1}) means free energy, the E value presents information about the mechanism of the adsorption process, describing whether adsorption is occurring chemically or physically; K_s (L μg^{-1}) and β represent Sips model constant and Sips model exponent, respectively.

2.5. Analysis of minimum selling price and CO_2 emissions in adsorbent production

The MSP of the adsorbent produced during ethanol production from FRs was estimated using several key assumptions. Fixed costs, capital depreciation, waste disposal, glucose for enzyme production, and other raw materials were assumed to be consistent with a LCB ethanol production process handling 773 tons per year, a report by the NREL.[22] Average income tax and return on investment were also applied based on this benchmark. Electricity was purchased for the pyrolysis of lignin and the production of bio-oil and biochar, as energy from the process was not used for self-supply. The mass balance of the process was considered to account for the co-production of ethanol, bio-oil, and biochar (adsorbent). Feedstock collection, processing, storage, and transport were assumed at $35 per dry ton.[23] By applying the market prices of sulfuric acid $130 per ton,[24] glycerol $335 per ton,[25] bio-oil

$486 per ton,[26] and ethanol $741 per ton,[26] the MSP of the adsorbent was determined. Glycerol loss was assumed to be 1% of the circulating glycerol 8 279 090 tons per year.

To determine CO_2 emissions from the biorefinery process, the Energy and Resources Group (ERG) Biofuel Analysis meta-Model (EBAMM) was used, specifically the version applied in the "Pimentel Switchgrass" analysis.[27] Two key assumptions were (1) electricity was purchased rather than generated onsite from the lignin byproduct, accounting for both process electricity and biomass grinding, and (2) heat was sourced from purchased natural gas instead of utilizing recovered waste heat from onsite lignin-fired electricity generation. CO_2 emissions were calculated to produce all biorefinery products, with economic allocation applied to distribute emissions between the co-products. The allocation was set at 30% for the adsorbent, 27% for bio-oil, and 44% for ethanol.[55]

3. Results and discussion

3.1. Surfactant-enhanced pretreatment fractionation and cellulose hydrolysis of FRs

The chemical composition and recovery rates of FRs subjected to surfactant-assisted acid/glycerol pretreatment at varying temperatures (100–160 °C) are shown in Table S1.† The analysis confirms that cellulose and lignin are the predominant components in the raw FRs, making up 48.9% and 47.6% of the dry weight, respectively, with only 2.1% xylan remaining due to the furfural production process, which removes most hemicellulose.[6] The ash content was found to be approximately 1.4%. These findings align with previous research showing typical compositions of FRs, which contain 40–50% lignin, 27–50% cellulose, and 2–5% xylan.[28] However, these variations can depend on the specific LCB source and methods used in FF production.[4]

Following pretreatment, increasing the pretreatment temperature (without surfactant) from 100 °C to 160 °C led to a decline in solid recovery (from 93.8% to 81.4%) and cellulose recovery (from 93.2% to 67.9%) (Table S1†), indicating that higher temperatures contribute to cellulose degradation. This observation alignside findings that increased temperatures (140–180 °C) during glycerol pretreatment degrade cellulose by 15% to 88%, depending on time.[13] The significant cellulose loss at higher temperatures is of concern for biofuel production, given cellulose's critical role in glucose generation. Regarding lignin, its content remained relatively stable (~48%) as the temperature increased from 100 °C to 140 °C but rose to 54.3% at 160 °C. This increase can be attributed to pseudo-lignin formation, a byproduct of cellulose degradation, accumulating on the substrate surface at high temperatures.[29]

Surfactant addition during pretreatment had notable effects on cellulose recovery, although it did not significantly impact lignin removal. Surfactants enhanced cellulose recovery by 0.5% to 4.9% at 100 °C and 3% to 8.4% at 120 °C (Table S1†). This improvement is likely due to surfactants reducing lignin redeposition, which protects cellulose from degradation and improves separation between lignin and cellulose.[14] High dosages of surfactants, such as 8% Tween 80 and 8% Triton X-100, improved delignification by approximately 5% in NaOH-catalyzed glycerol pretreatment of sugarcane bagasse.[9] However, a similar effect was not observed in the current study.

To further evaluate the impact of pretreatment on FRs fractionation, cellulose hydrolysis (solid loading: 2% (w/v), enzyme loading: 8 FPU g^{-1}) was conducted on all pretreated samples. As shown in Fig. 2, both temperature and the presence of surfactant in pretreatment significantly influenced glucose yields. Cellulose hydrolysis efficiency increased with rising temperatures for 24 h and 48 h. At 100 °C, relatively modest glucose yields of 34.1% (24 h) and 49.9% (48 h) were recorded, while higher yields were observed at elevated temperatures, highlighting improved fractionation at elevated temperatures. The reduction in cellulose recovery at higher temperatures (140 °C: 79.7% cellulose recovery; 160 °C: 67.9% cellulose recovery) concentrated the residual cellulose, allowing the same enzyme loading to work more effectively and leading to higher glucose production.[13]

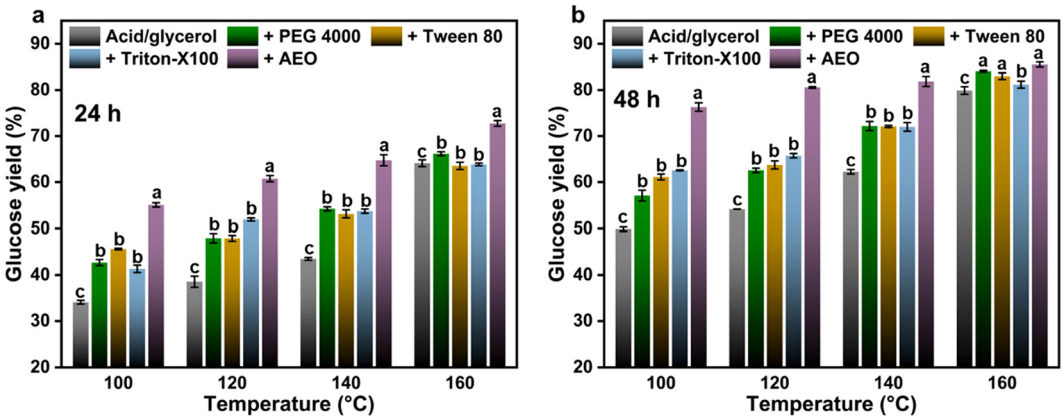

Fig. 2 Cellulose hydrolysis of acid/glycerol pretreated FRs (without/with surfactant) at varying temperatures. Solid loading: 2% (w/v); Enzyme loading: 8 FPU g^{-1}; Hydrolysis time: 24 h (a) and 48 h (b).

Without surfactants, pretreatment at 160 °C yielded 64.0% glucose after 24 h of hydrolysis. However, with surfactants, the yields improved significantly. For example, PEG 4000 increased glucose yield to 66.1% after 24 h and 84% after 48 h. Similarly, Tween 80 boosted yields, though not as substantially as PEG 4000. Triton X-100 showed moderate improvements, while AEO consistently delivered the highest glucose yields, reaching 72.7% at 24 h and 85.5% at 48 h. Among the tested surfactants, AEO demonstrated the most significant enhancement in glucose yield, likely due to its ability to reduce surface tension and improve enzyme accessibility by solubilizing hydrophobic components, allowing more efficient interaction with cellulose fibers.[14] This surfactant's capacity to create a more enzyme-friendly environment explains its superior performance to other surfactants.[30] Additionally, the impact of varying AEO dosages on chemical composition and hydrolysis yields is summarized in Table S2.† While increasing the AEO dosage from 1% to 7% did not markedly alter the chemical composition, it significantly improved cellulose hydrolysis yields, which rose from 72.2% at 1% AEO to 85.5% at 5% AEO, peaking at 84.1% with 7% AEO. The underlying mechanisms driving this improvement will be discussed further in section 3.2.

In summary, temperature and surfactant addition play pivotal roles in enhancing glucose yields from cellulose hydrolysis of pretreated FRs. Considering the criteria of maximum cellulose recovery (96.6%) and high hydrolysis yield (without AEO: 54.1%; with 5% AEO: 85.5%), the optimal pretreatment conditions were determined to be 120 °C with 5% AEO.

3.2. Modification in physicochemical characteristics of surfactant-driven pretreated FRs

To elucidate the influence of AEO on the acid/glycerol pretreatment of FRs, a comprehensive characterization of the optimally pretreated FRs was conducted using FTIR, CrI, pore characteristics, and SEM analyses (Fig. 3). These analyses provide critical insights into the physicochemical transformations that underpin the enhanced cellulose hydrolysis observed. The FTIR spectra of raw and pretreated FRs (without/with AEO) demonstrate significant chemical modifications that can contribute to improving biomass accessibility (Fig. 3a). A pronounced peak at 3310 cm^{-1}, corresponding to the stretching vibrations of hydroxyl (O–H) groups in cellulose,[14] in which pretreated FRs in particular in the presence of AEO, observed relatively slightly stronger peaks than that in raw FRs. Additional changes are evident in the C–H vibration bands of cellulose at 2922 cm^{-1}, which show heightened intensity in both pretreated FRs, suggesting more available cellulose for further cellulose hydrolysis. Alterations specific to lignin are observed in the 1690 cm^{-1} and 1575 cm^{-1} peaks, corresponding to C═O and C–C stretching and the aromatic skeleton of lignin, respectively. The persistence of these peaks after pretreatment reflects the partial disruption of lignin's

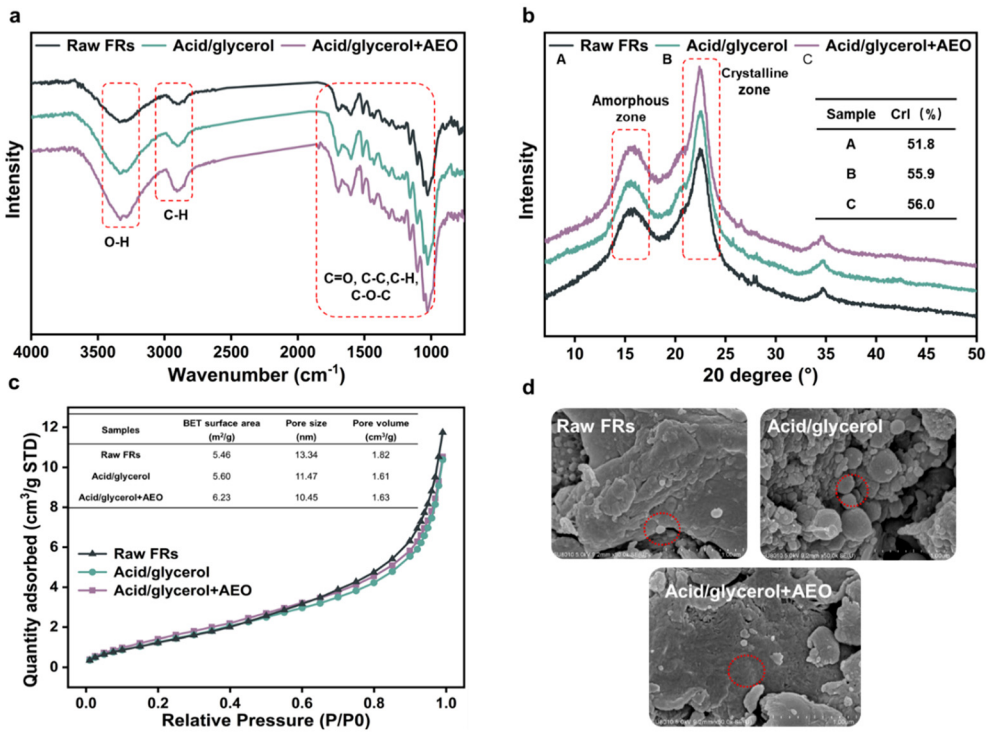

Fig. 3 Physicochemical characteristics of raw and pretreated FRs (without/with AEO). FTIR analysis (a), XRD patterns (b), pore properties (c), and SEM (d).

complex network. Furthermore, the intensity of the bond at 1014 cm^{-1}, associated with the asymmetric stretching of C–O–C linkages between cellulose and lignin, is significantly reduced in the pretreated samples. This reduction indicates a weakening of cellulose-lignin interactions, a key factor in improving cellulose accessibility and enhancing hydrolysis efficiency.

The CrI of biomass plays a pivotal role in cellulose hydrolysis efficiency.[5] Notably, the intensities of both amorphous and crystalline regions increased following pretreatment (Fig. 3b). The CrI of raw FRs was measured at 51.8%, rising to 55.9% in pretreated FRs without AEO and to 56.0% with AEO. This marginal increase suggests that the presence of AEO during pretreatment has a negligible impact on cellulose crystallinity. The minimal variation in crystallinity implies that the primary mechanism behind improved cellulose hydrolysis is likely linked to the disruption of lignin-cellulose interactions rather than significant alterations in substrate crystallinity.[31]

The raw FRs exhibited a BET surface area of 5.46 $m^2\ g^{-1}$, a pore size of 13.34 nm, and a pore volume of 1.82 $cm^3\ g^{-1}$. After acid/glycerol pretreatment, these values showed slight changes, with the BET surface area increasing marginally to 5.60 $m^2\ g^{-1}$, while the pore size and pore volume dropped to 11.47 nm and 1.61 $cm^3\ g^{-1}$, respectively (Fig. 3c). This reduction in pore size, alongside a decreased pore volume, suggests the restructuring of the pore network, possibly due to partial collapse or reorganization of mesopores during pretreatment.[9] However, with the inclusion of AEO in pretreatment, a more pronounced improvement in porosity was observed. The BET surface area increased to 6.23 $m^2\ g^{-1}$, the pore size further reduced to 10.45 nm, and the pore volume slightly rose to 1.63 $cm^3\ g^{-1}$. The reduction in pore size, combined with an increase in surface area, indicates that AEO likely facilitates the development of more microporous structures, which could enhance enzyme accessibility and improve hydrolysis efficiency. Overall, the AEO-assisted pretreatment led to a more refined pore structure, as reflected in the improved surface characteristics of the pretreated FRs.

Additionally, alterations in surface morphology were assessed through SEM (Fig. 3d). The raw FRs exhibited a compact, smooth surface characterized by small, spherical droplets, with a notable increase in droplet density on the surfaces of the pretreated FRs. As documented in numerous studies, the formation of these droplets, often referred to as pseudo-lignin, arises from the partial degradation of lignin and cellulose under acidic pretreatment conditions, thereby reducing the available surface area for enzyme interaction with cellulose.[32] Remarkably, pretreated FRs containing AEO displayed a clean surface devoid of droplet formation. This observation suggests that incorporating AEO during pretreatment may mitigate pseudo-lignin formation, thereby enhancing the accessible surface area for enzyme interactions with cellulose.

Based on the results of the physicochemical characterization, the enhanced cellulose hydrolysis observed in the AEO-assisted pretreatment can be attributed to the weakening of cellulose-lignin interactions, improved surface properties, and prevention of pseudo-lignin formation, all of which contribute to increased enzyme accessibility and hydrolysis efficiency.

3.3. Ethanol production through high-solid cellulose hydrolysis and fermentation

Due to the high lignin content in the pretreated FRs (48.6% without AEO; 48.2% with AEO), the SHF method was applied to maximize cellulose conversion to ethanol. A fed-batch hydrolysis process was employed, starting with 8% solid loading, with additional feedings of 4% at 6, 12, and 24 h to achieve a final solids loading of 20%, following an established protocol.[13] Fed-batch hydrolysis was used to improve enzyme accessibility and mixing efficiency by gradually increasing solid loadings, reducing viscosity, and substrate inhibition.[19] This approach optimizes glucose yields while maintaining efficient hydrolysis under high-solid conditions.[19,53]

As a result, the hydrolysis over 48 h yielded high glucose concentrations: 49.3 g L^{-1} (48.4% conversion) from FRs without AEO (Fig. 4a) and 84.7 g L^{-1} (79.9% conversion) from FRs with AEO (Fig. 4b). Extending the hydrolysis time to 72 h resulted in only a slight increase in glucose yield. The highest glucose titers and yields were observed for FRs pretreated with AEO, achieving 87.5 g L^{-1} with an 82.5% yield, compared to 52.6 g L^{-1} and 51.6% yield for FRs without AEO. Remarkably, the presence of AEO resulted in a 37.4% increase in glucose yield, a significant improvement attributed to enhanced porosity and reduced pseudo-lignin formation in the pretreated FRs (Fig. 3). In our previous study, using 20% solid loading and an enzyme dosage of 15 FPU g^{-1} with the fed-batch method, reported glucose yields ranging from 80% to 86.8%,[13] suggesting that AEO-assisted pretreatment could substantially reduce enzyme costs. Moreover, the glucose yields achieved in this study with high-solids cellulose hydrolysis were considerably higher than those reported in earlier studies, which showed yields ranging from 18.6% to 99.5%, depending on FRs loading (2%–20%) and enzyme dosages (6.7–30 FPU g^{-1}) for various pretreated FRs.[6]

Regarding ethanol production, 90% of the glucose was consumed within the first 24 h of fermentation, with nearly complete conversion to ethanol within 36 h. This rapid glucose uptake indicates a brief 1 to 2 h lag for the *S. cerevisiae* Angel strain, enabling efficient ethanol production.[33] The highest ethanol titers were achieved from pretreated FRs, yielding 22.0 g L^{-1} without AEO and 36.6 g L^{-1} with AEO, corresponding to ethanol yields of 0.12 g g^{-1} and 0.20 g g^{-1}, respectively (Table S3†). In comparison, previous studies using alkaline peroxide- and glycerol-pretreated FRs reported lower ethanol titers of 16 g L^{-1} and 27.8 g L^{-1}, respectively,[13] likely due to lower glucose availability during hydrolysis and the constraints of the simultaneous saccharification and fermentation (SSF) method, which is particularly sensitive to the inhibitory effects of elevated lignin content.[33]

Ethanol productivities for FRs without and with AEO pretreatment were 1.31 g $L^{-1}\ h^{-1}$ and 2.38 g $L^{-1}\ h^{-1}$, respectively (Table S3†). In industrial ethanol production, productivity values between 0.98 g $L^{-1}\ h^{-1}$ and 2.47 g $L^{-1}\ h^{-1}$ are often

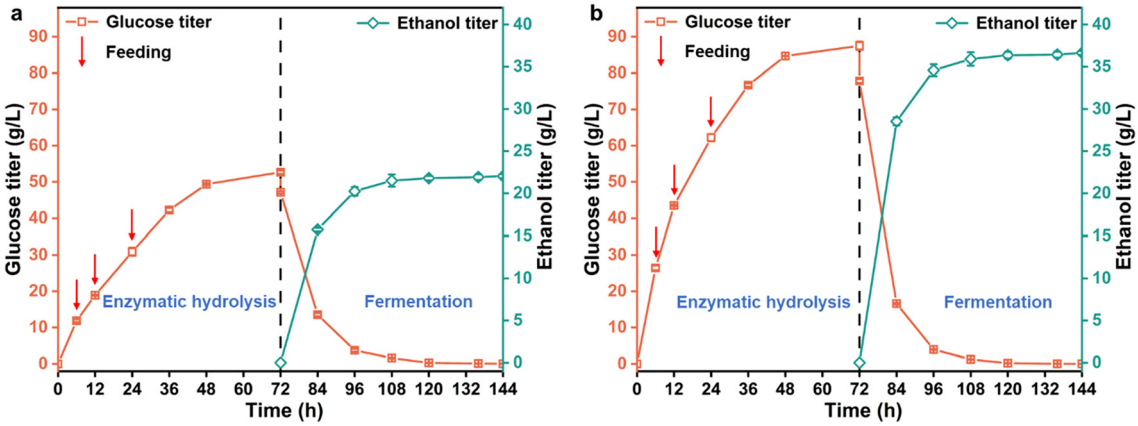

Fig. 4 High-solid cellulose hydrolysis of pretreated FRs without (a) and with (b) AEO to produce ethanol. Total solid loading: 20% (w/v); Enzyme loading: 8 FPU g^{-1}; Hydrolysis time: 72 h; Fermentation time: 72 h.

considered efficient, with higher values indicating strong fermentation performance.[6] The 2.38 g L^{-1} h^{-1} achieved with AEO-assisted pretreatment demonstrates impressive productivity, suggesting that the pretreatment effectively enhances the fermentation process. This would be promising for scaling up and improving the economic viability of ethanol production processes.[9] Moreover, the theoretical maximum ethanol yields for pretreated FRs without and with AEO were 91.1% and 91.4%, respectively, highlighting the significant potential of this process in ethanol production (Table S3†).

3.4. Thermolysis analysis and pyrolysis products of FRs' lignin without/with AEO

Thermal decomposition, as evaluated through TG/DTG analysis, provides essential insights into the degradation mechanisms of structural FRs during pyrolysis. In this study, TG/DTG methods were applied to both raw FRs (as control) and remaining residues after cellulose hydrolysis (without/with AEO) to examine variations in their thermal degradation profiles (Fig. 5). Mass loss in all samples was primarily associated with the release of gases and volatile compounds at elevated temperatures (Fig. 5a). The TG curves demonstrated a progressive decrease in lignin mass with rising temperature, while the DTG curves depicted the rate of this mass loss, revealing three distinct phases of thermal behavior.[34]

In the initial phase (up to 250 °C), moderate weight loss occurred, primarily due to dehydration and the release of low-molecular-weight volatiles.[13] This phase is critical as it reflects the samples' moisture content and initial volatile components. The second phase, characterized by active pyrolysis (250–500 °C),[35] exhibited a marked mass reduction, with raw FRs showing a steeper decline than the pretreated samples. This suggests that pretreatment enhances thermal stability by reducing the release of volatile matter during thermolysis.[35] In the final phase, beyond 500 °C, the char formation stage highlighted the residual mass after thermolysis, reflecting the structural integrity of the treated samples.[35] The final biochar yields at 800 °C were 28.5% for raw FRs and 37.5% and 34.4% for lignin without and with AEO, respectively. This is particularly relevant for applications where biochar serves as a valuable byproduct or a stabilizing agent in various formulations.[36] DTG analysis (Fig. 5b) identified distinct peaks corresponding to mass loss rates, with significant points at 355.4 °C for lignin without AEO and raw FRs, while the lignin-containing AEO peaked at 367.8 °C. The shift in peak temperature with AEO suggests that its incorporation not only influences the decomposition temperature but also enhances the overall thermal stability of the lignin.[37] This enhancement in thermal stability holds significant potential for use in producing transportation fuels, commercial chemicals, and functional materials, where the thermal behavior of lignin plays a crucial role.[37]

Pyrolysis was conducted on raw FRs and lignin samples (without/with AEO), resulting in three primary products: crude bio-oil, biochar, and syngas (Fig. 5c). The temperature significantly influenced the pyrolysis process, with the optimal bio-oil yield achieved at 550 °C, a key condition for maximizing liquid production while minimizing solid residue formation.[13] The highest bio-oil yield of 39.2% was obtained from lignin samples with AEO, followed by lignin without AEO (34.8%) and raw FRs (33.8%). The relatively high bio-oil yield from raw FRs can be attributed to cellulose and lignin. Remarkably, lignin samples with AEO showed an 11.2% increase in bio-oil yield relative to those without AEO, suggesting that AEO may modify or activate lignin, enhancing its conversion to bio-oil. Similar studies on PEG-aided glycerol lignin from sugarcane bagasse reported a 58% improvement in bio-oil yield, which was linked to the protection of β-O-4 and formation of new β-O-4′ linkages in lignin *via* PEG.[12] Compared to previous work where acid/glycerol lignin from FRs produced a 28% bio-oil yield, this study reports a 17% increase (34.8%),[13] attributed to differences in LCB source and FF production techniques.

The biochar yields from lignin samples (without/with AEO) were comparable, with values of 50.6% and 51.0%, respect-

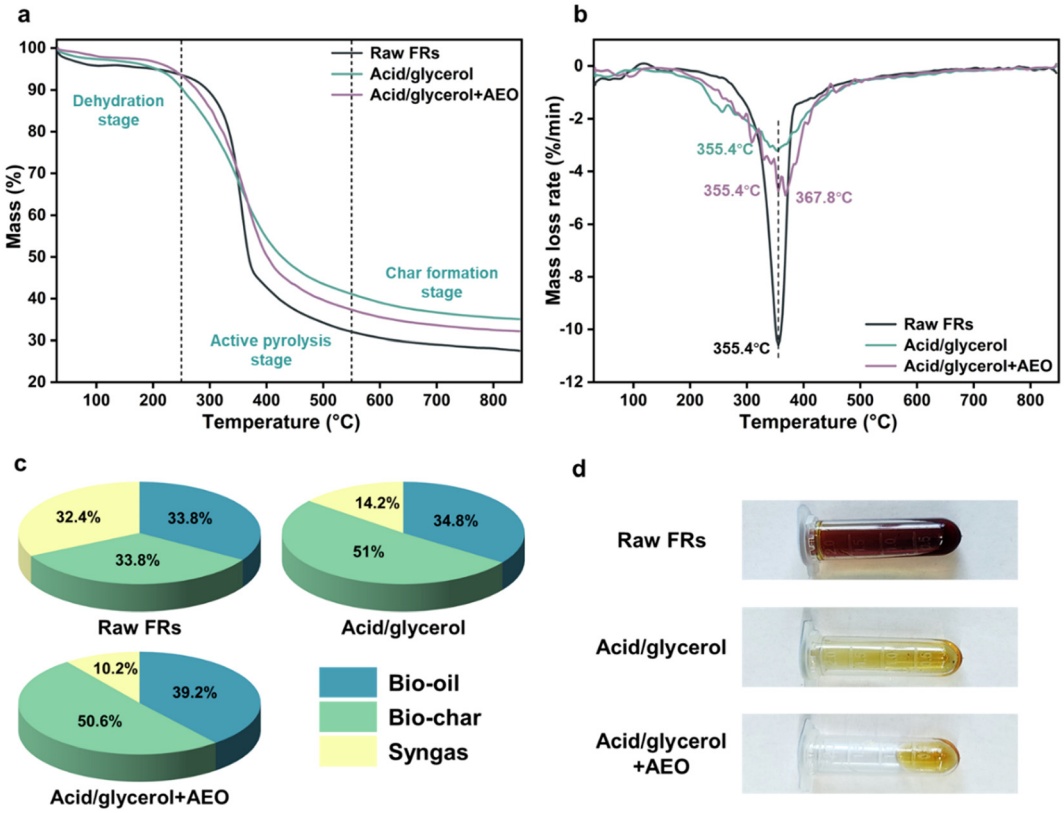

Fig. 5 TG (a) and TGD (b) curves of raw FRs (control) and lignin samples (without/with AEO) after thermolysis. Product distribution yields (c) and image of bio-oil after pyrolysis of raw FRs (control) and lignin samples (without/with AEO) (d).

ively, while raw FRs generated 33.8% biochar, reflecting a trend similar to that observed in the TG analysis. Syngas production displayed an inverse trend, with raw FRs yielding 32.4% syngas, which decreased to 14.2% for lignin without AEO and further to 10.2% with the addition of AEO. This reduction in syngas output suggests enhanced bio-oil and biochar production occurs at the expense of syngas formation.[38] Furthermore, the lighter color of the bio-oil from lignin samples with and without AEO (Fig. 5d) compared to raw FRs bio-oil indicates the presence of fewer undesirable high-molecular-weight compounds, a hypothesis that will be confirmed in the bio-oil characterization (section 3.5).

3.5. Bio-oil compositions of FRs' lignin without/with AEO

Fig. 5 presents the principal chemical functionalities identified in bio-oil fractions obtained from lignin pyrolysis at 550 °C. Both the acid/glycerol method and AEO profoundly affected the composition of the bio-oil, particularly in modulating the distribution and diversity of chemical compounds produced. Phenolic compounds emerged as the predominant products across the bio-oil fractions, with their relative abundance increasing from raw FRs (8.4%) to lignin without AEO (28.1%) and further to AEO-assisted lignin (30.9%) (Fig. 6a). This increase mirrors findings in previous research, such as PEG-assisted glycerol lignin from sugarcane bagasse, which showed a 61.0% rise in aromatic content due to the preservation of β-O-4 linkages in the lignin structure.[9,12]

GC/MS analysis provided more profound insights into the composition of the bio-oil. The major constituents identified in bio-oil from raw FRs were (**1**) Ethanone, 1-(1-cyclohexen-1-yl)-, (**2**) Phenol, 2,6-dimethoxy-, (**3**) Phenol, (**4**) Furfural, (**5**) Phenol, 4-ethyl-, (**6**) *p*-Cresol, (**7**) 1,2-Cyclopentanedione, 3-methyl-, and (**8**) 2-Furancarboxaldehyde, 5-methyl- (Fig. 6b). For lignin without AEO, the dominant compounds were (**1**) Phenol, 4-ethyl-2-methoxy-, (**2**) Phenol, 2-methoxy-, (**3**) Phenol, 4-ethyl-, (**4**) Phenol, (**5**) 2-Methoxy-4-vinylphenol, (**6**) Phenol, 2,6-dimethoxy-, and (**7**) Creosol (Fig. 6c). Lignin containing AEO, the composition shifted slightly, with essential products being (**1**) Phenol, 4-ethyl-2-methoxy-, (**2**) Phenol, 4-ethyl-, (**3**) Phenol, 2-methoxy-, (**4**) Phenol, (**5**) Creosol, (**6**) Phenol, 2,6-dimethoxy-, (**7**) 2-Methoxy-4-vinylphenol, (**8**) 4-Vinylphenol, and (**9**) 3,5-Dimethoxy-4-hydroxytoluene (Fig. 6d). The phenolic compounds identified in the bio-oil are of particular interest due to their wide-ranging applications across various industries.[39] For example. Phenol, 4-ethyl-2-methoxy-, a guaiacol derivative, is valuable for synthesizing fine chemicals, adhesives, and polymers known for their high thermal stability.[39] Phenol, 4-ethyl- and phenol, 2-methoxy- (guaiacol) serve as important intermediates for producing bio-based antioxidants, synthetic rubbers, and vanillin, which is widely used in the food, fragrance, and pharmaceutical sectors.[39] Creosol and

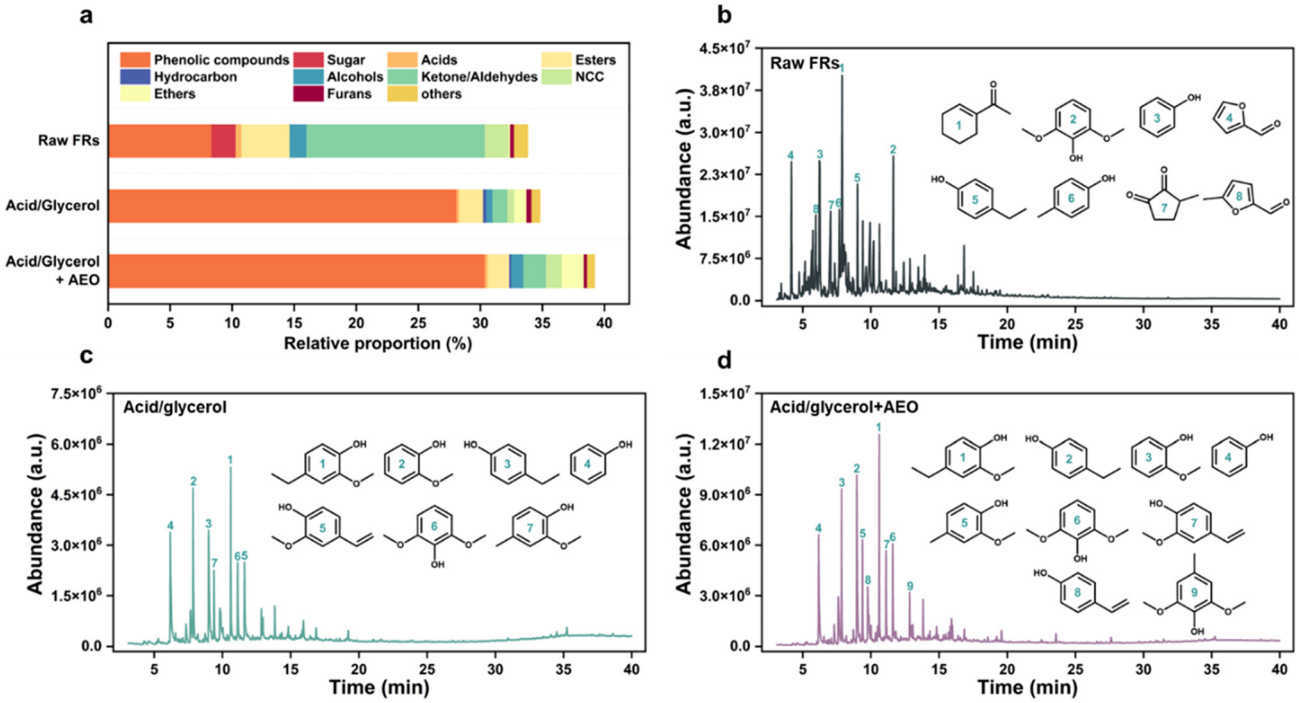

Fig. 6 Relative percentage of bio-oil composition (a) and their peaks in the raw FRs (b), lignin sample without AEO (c), and with AEO (d) using GC/MS analysis.

2-Methoxy-4-vinylphenol are key compounds for wood preservatives and fragrances, with potential for application in bio-based polymer production.[39] Furthermore, 4-Vinylphenol and 3,5-Dimethoxy-4-hydroxytoluene are critical for developing high-performance resins and biodegradable plastics, contributing to the sustainable materials industry.[40]

The findings underscore pretreatment's critical role in fine-tuning bio-oil's chemical profile. AEO-assisted pretreatment, in particular, proved effective in enriching the yield of valuable phenolic compounds, highlighting its potential for optimizing bio-oil composition. This enhancement is crucial for biorefinery operations that produce renewable chemicals and high-value materials, thereby contributing to developing sustainable, circular economies.

3.6. Adsorption performance of PFOA on biochar

Biochar produced from FRs through pyrolysis exhibits remarkable potential as an adsorbent for environmental pollutants, particularly PFOA. Characterized by a high surface area, developed porosity, and abundant functional groups, this biochar effectively sequesters PFOA, a persistent organic pollutant associated with severe health and environmental risks.[41] This section examines the adsorption performance of PFOA on biochar, focusing on the adsorption dynamics and unveiling the adsorption mechanism through the physicochemical characterization of biochar samples before and after PFOA adsorption. These insights underscore the potential of FRs-derived biochar as a sustainable solution for environmental remediation, offering a viable pathway to valorize industrial byproducts in pollution mitigation efforts.

3.6.1. Adsorption dynamics of PFOA on biochar samples. The biochar samples derived from raw FRs and acid/glycerol + AEO post-pyrolysis were evaluated for their PFOA adsorption potential. To understand the adsorption behavior, kinetic studies were conducted using both the pseudo-first-order and pseudo-second-order models, while the adsorption isotherms were assessed using four models: Langmuir, Freundlich, Dubinin–Radushkevich, and Sips (Fig. 7). The adsorption dynamics indicated that PFOA was rapidly adsorbed within the first 12 h, with equilibrium being approached by 24 h (Fig. 7a and b).

The pseudo-second-order model yielded correlation coefficients (R^2) exceeding 0.98 for both biochar samples, considerably higher than those for the pseudo-first-order model (0.93 for raw FRs and 0.94 for acid/glycerol + AEO biochar) (Table 1). Moreover, the theoretical adsorption capacities derived from the pseudo-second-order model were in close agreement with the experimental results, suggesting that this model better describes the adsorption kinetics, implying that chemical sorption is the primary mechanism governing PFOA uptake.[21]

For the adsorption isotherms, the Dubinin–Radushkevich and Sips models provided the best fits, as indicated by their superior R^2 values compared to the other models (Fig. 7c, d and Table 2). The maximum theoretical adsorption capacities (Q_S) of PFOA on raw FRs biochar were 30 953.82 μg g^{-1} (Dubinin–Radushkevich) and 30 934.41 μg g^{-1} (Sips). In contrast, these capacities were lower for the acid/glycerol + AEO

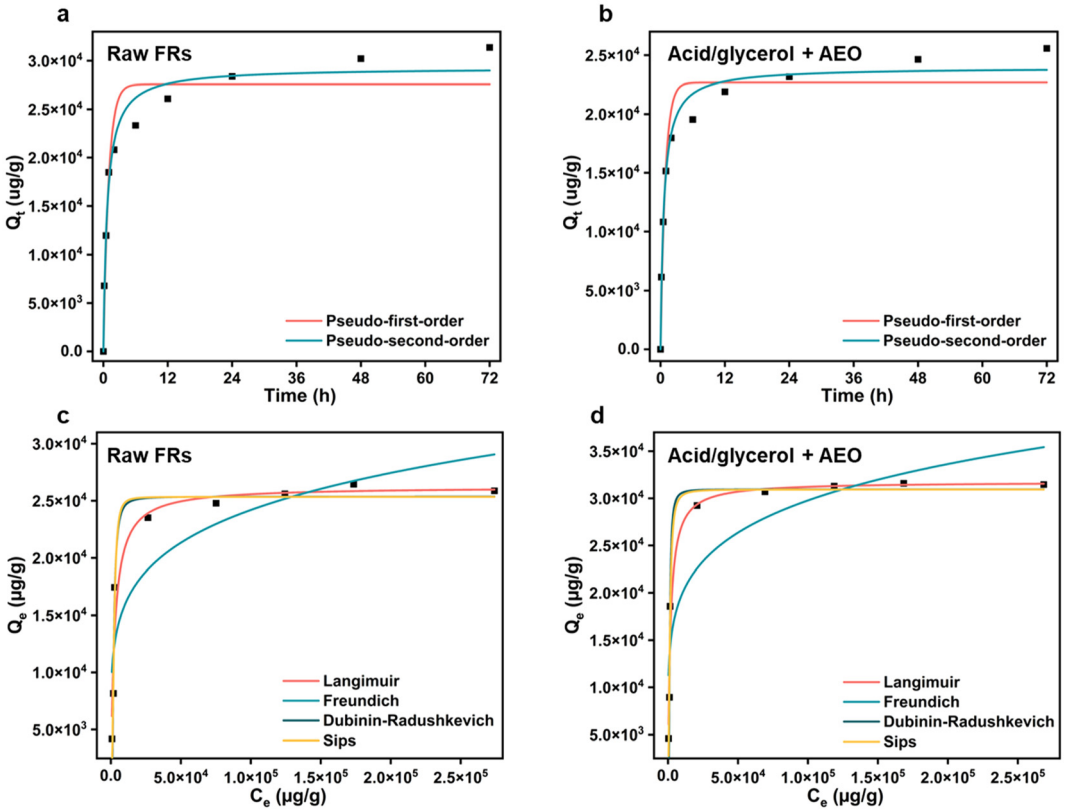

Fig. 7 Adsorption model fitting curves of PFOA on biochar samples. The pseudo-first-order and pseudo-second-order model fitting curves of raw FRs (a) and acid/glycerol + AEO biochars (b). Langmuir, Freundlich, Dubinin–Radushkevich, and Sips model fitting curves of (c) raw FRs and (d) acid/glycerol + AEO biochar. (Initial concentrations: 35 000 μg g^{-1}, additional 1.0 g L^{-1}, pH 7.0 ± 0.2).

Table 1 Isotherm factors of PFOA adsorption on biochar samples

Biochar samples	Model type	Factors	Target pollution PFOA
Raw FRs	Pseudo-first-order	Q_{c1} (μg g^{-1})	27 573.81
		K_1 (h^{-1})	1.03
		R^2	0.93
	Pseudo-second-order	Q_{c2} (μg g^{-1})	29 269.69
		K_1 (h^{-1})	4.82×10^{-5}
		R^2	0.98
Acid/glycerol + AEO	Pseudo-first-order	Q_{c1} (μg g^{-1})	22 681.07
		K_1 (h^{-1})	1.13
		R^2	0.94
	Pseudo-second-order	Q_{c2} (μg g^{-1})	23 952.29
		K_1 (h^{-1})	6.78×10^{-5}
		R^2	0.98

biochar, at 25 363.94 μg g^{-1} and 25 342.12 μg g^{-1}, respectively, closely matching experimental data. This reduced adsorption capacity in the treated biochar might be attributed to the absence of cellulose, as the acid/glycerol + AEO biochar consisted only of lignin, unlike the raw FRs biochar, which contained both lignin and cellulose. Further physicochemical characterization will explore the structural differences responsible for this variation in adsorption performance. Moreover, PFOA's free energy values (E) were all less than 8 kJ mol^{-1}, indicating that the adsorption predominantly involved physical sorption mechanisms.[21] Additionally, the Sips exponent values ($\beta > 1$) suggest that the adsorption process is driven by surface heterogeneity, with active sites exhibiting varying affinities for PFOA.[21] This finding highlights the complexity of the adsorption mechanism, which likely involves both physical and chemical interactions at the biochar surface.

In conclusion, the adsorption of PFOA on biochar samples is governed by a combination of heterogeneous physical sorption and chemical sorption processes, with the pseudo-second-order model and the Dubinin–Radushkevich and Sips isotherms providing the most accurate representations of the adsorption dynamics and capacities.

3.6.2. Physicochemical properties of biochar pre- and post-PFOA adsorption. Elemental analysis of the biochar samples revealed notable differences in their composition, which are crucial for understanding their effectiveness in environmental applications, particularly in contaminant adsorption.[21] Table 3 details the pH level and elemental composition of biochar samples. The acid/glycerol + AEO biochar exhibited a higher pH (8.0) compared to raw FRs biochar (7.2), indicating that it might be more suited for specific adsorption applications where primary conditions are favorable.[42] Additionally, the carbon (C) content was markedly higher in the raw FRs biochar (81.0%) compared to the acid/glycerol + AEO biochar (52.2%). This elevated carbon content in the raw biochar

Table 2 Kinetic factors of PFOA adsorption on biochar samples

Biochar samples	Model type	Factors	Target pollution PFOA
Raw FRs	Langmuir	Q_m (μg g^{-1})	31 743.92
		k_L (L μg^{-1})	5.90×10^{-4}
		R^2	0.95
	Freundlich	k_f ($\mu g^{1-1/n}$ g^{-1} $L^{1/n}$)	3930.63
		$1/n$	0.176
		R^2	0.79
	Dubinin–Radushkevich	Q_s (μg g^{-1})	30 953.82
		K_{dr} (mol^2 J^{-2})	0.199
		R^2	0.96
	Sips	Q_{ms} (μg g^{-1})	30 934.41
		k_s (L μg^{-1})	7.42×10^{-4}
		β	1.912
		R^2	0.96
Acid/glycerol + AEO	Langmuir	Q_m (μg g^{-1})	26 229.45
		k_L (L μg^{-1})	3.89×10^{-4}
		R^2	0.93
	Freundlich	k_f ($\mu g^{1-1/n}$ g^{-1} $L^{1/n}$)	2981.61
		$1/n$	0.182
		R^2	0.77
	Dubinin–Radushkevich	Q_s (μg g^{-1})	25 363.94
		K_{dr} (mol^2 J^{-2})	0.520
		R^2	0.94
	Sips	Q_{ms} (μg g^{-1})	25 342.12
		k_s (L μg^{-1})	4.4985×10^{-4}
		β	2.589
		R^2	0.99

Table 3 pH and elemental distribution of biochar samples

Biochar samples	pH	N	C	H	S	O	H/C	O/C	(N + O)/C
Raw FRs	7.2	1.7	81.0	3.4	0.1	13.8	0.04	0.2	0.2
Acid/glycerol + AEO	8.0	1.0	52.2	2.2	1.3	43.4	0.04	0.8	0.9

suggests a larger surface area and greater potential for adsorption.[21] The nitrogen (N) content of the raw FRs biochar was also slightly higher (1.7%) than that of the acid/glycerol + AEO biochar (1.0%), which could enhance its capacity to bind organic contaminants, thereby improving its adsorption efficiency.[43] Despite both samples exhibiting the same H/C ratio (0.04), indicating comparable hydrogen content, the O/C ratio in the acid/glycerol + AEO biochar was significantly higher (0.8). This elevated O/C ratio suggests greater functionalization, enhancing the biochar's chemical reactivity and interaction potential.[43] Furthermore, the (N + O)/C ratio, a critical indicator of chemical interaction capacity, was higher in the acid/glycerol + AEO biochar (0.9), highlighting its improved potential for chemical sorption processes.[44]

Pore characterization has revealed that biochar samples' surface area and porosity play a crucial role in their ability to adsorb contaminants. BET analysis demonstrated that raw FRs biochar exhibited a surface area of 98.3 m^2 g^{-1} and a total pore volume of 11.4 cm^3 g^{-1}, both of which were higher than those of the acid/glycerol + AEO biochar (Fig. 8a). The smaller average pore diameter of 3.7 nm in raw FRs biochar further enhances its capacity to adsorb smaller molecules, making it particularly effective for capturing contaminants like PFOA.[17] This observation aligns with the findings from kinetic and adsorption isotherm studies, where higher adsorption rates were noted with raw FRs biochar (Fig. 7). The larger surface area and pore volume of raw FRs biochar provide an increased number of active sites, facilitating enhanced interactions with PFOA molecules.[20] This structural advantage promotes the efficient diffusion of PFOA into the biochar's pores, significantly boosting its overall adsorption capacity.[43] Furthermore, SEM images after PFOA adsorption revealed a smoother surface on the raw FRs biochar, suggesting that its morphology may contribute to improved adsorption potential (Fig. 8a).

XPS analysis provided clear evidence of PFOA adsorption, confirmed by the detection of fluorine (F 1s) peaks in the spectra (Fig. 8b). Significant changes were observed in the high-resolution C 1s and O 1s spectra before and after the adsorption process (Fig. 8c). In the case of the raw FRs biochar, the C 1s spectrum initially showed a dominance of C–C/C=C bonds, making up 72.3% of the total carbon species before PFOA adsorption, along with C–O groups at 21.2% and C=O groups at 6.5%. Following adsorption, the proportion of C–C/C=C bonds slightly increased to 73.7%, indicating a possible stabilization of these structures as they interacted with PFOA.[20] In contrast, the C–O and C=O groups decreased to 19.2% and 7.0%, respectively, suggesting that these functional groups actively participated in adsorption, promoting interactions with PFOA.[44] For the O 1s spectrum of raw FRs biochar, a reduction in O–C=O groups was observed, dropping from 36.7% to 33.0% after PFOA adsorption, while the C–O content increased from 30.8% to 36.2%. This shift suggests PFOA adsorption altered the surface chemistry, likely enhancing the biochar's binding affinity to the contaminant *via* the available C–O sites.[44]

In contrast, the acid/glycerol + AEO biochar initially showed a C 1s composition consisting of 79.0% C–C/C=C bonds, 13.8% C–O groups, and 7.1% C=O groups. After PFOA adsorption, the C–C/C=C content decreased to 74.8%, while the C–O groups increased to 18.6%, and C=O slightly reduced to 6.5%. This change implies that the interaction with PFOA disrupted the stable C–C structures, making more C–O groups available for binding, thus improving adsorption efficiency.[45] The O 1s spectrum for this biochar sample remained relatively stable, with O–C=O groups showing a slight increase from 41.4% to 47.4% after adsorption. This stability indicates that oxygen-containing functional groups in the biochar were preserved, potentially enhancing its capacity to interact with PFOA and other contaminants. Overall, the XPS analysis revealed dynamic alterations in the surface chemistry of both biochar samples during PFOA adsorption. The raw FRs biochar demonstrated stabilization of C–C/C=C structures, while the acid/glycerol + AEO biochar showed increased availability of C–O and O–C=O groups, pointing to different interaction mechanisms with PFOA. These findings highlight the critical role of functional group dynamics in boosting biochar's adsorption capacity, reinforcing its potential for effective environmental remediation.

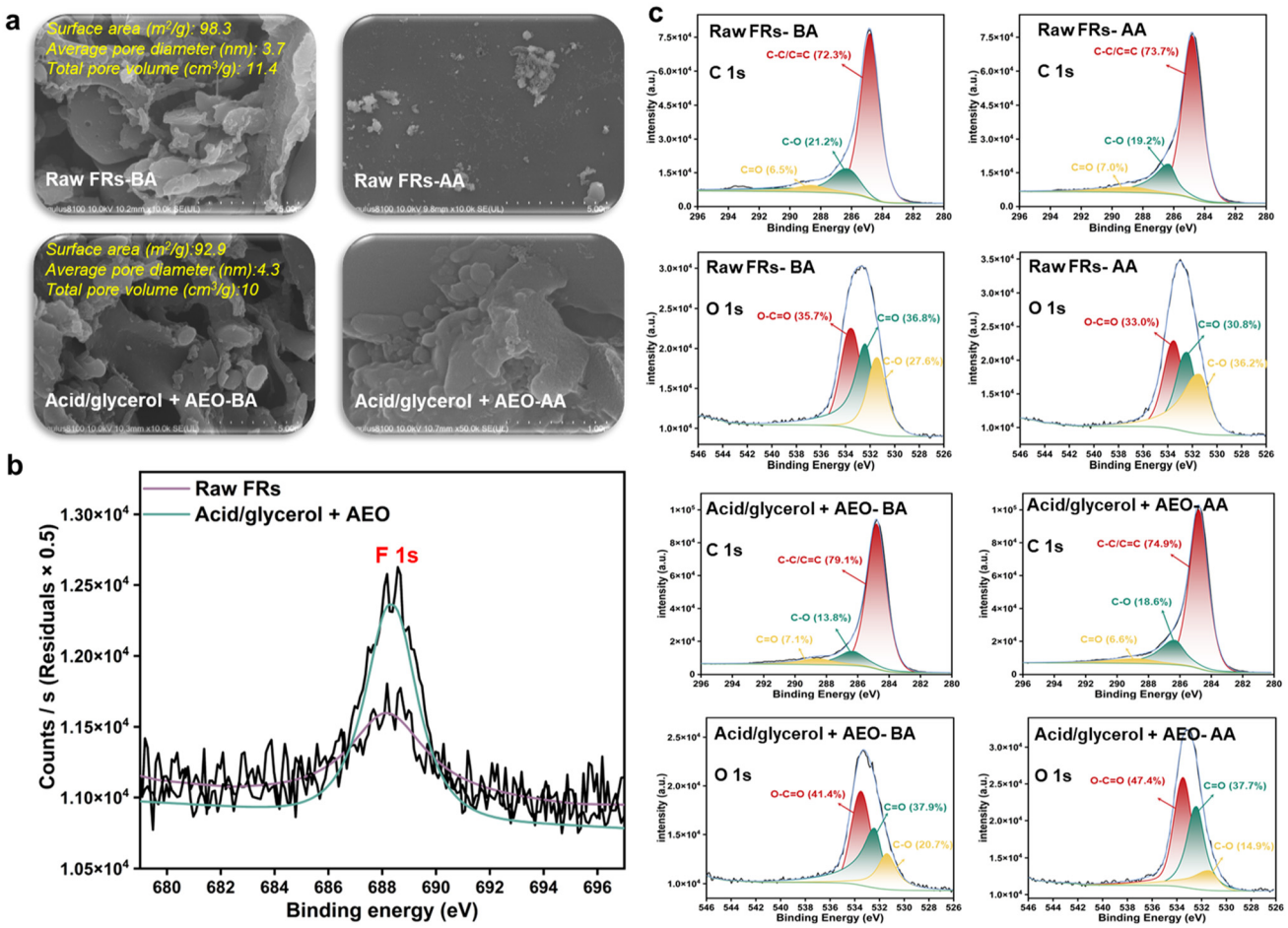

Fig. 8 BET, surface images (SEM) (a), and XPS spectra (b) along with C 1s and O 1s of biochar samples (c). BA: before adsorption; AA: after adsorption.

3.6.3. Mechanism of PFOA adsorption on biochar samples. The adsorption of PFOA on biochar surfaces is governed by a complex interplay of mechanisms influenced by the distinct physicochemical properties of each biochar (Fig. 9a). Electrostatic interactions are crucial, as the negatively charged carboxylate group of PFOA interacts with positively charged sites on the biochar.[21] Both raw FRs and acid/glycerol + AEO biochars contain functional groups like carboxyl and hydroxyl that can become protonated under certain pH conditions, enhancing electrostatic attraction toward PFOA molecules.[21] Hydrogen bonding also plays a significant role, facilitated by the presence of polar functional groups such as hydroxyl (–OH), carboxyl (–COOH), and carbonyl (C═O) on the biochar surfaces.[20] Due to its chemical modification, the acid/glycerol + AEO biochar has a higher density of oxygen-containing groups, enabling more extensive hydrogen bonding compared to raw FRs biochar, which enhances its adsorption capacity. Hydrophobic interactions are another key mechanism driven by the hydrophobic nature of PFOA's fluorinated tail.[46] Both biochars' aromatic and aliphatic structures provide hydrophobic domains that promote adsorption through van der Waals forces. Raw FRs biochar, with a higher content of stable C–C/C═C bonds, exhibits stronger hydrophobic interactions than acid/glycerol + AEO biochar, which has more hydrophilic C–O groups. This is reflected in contact angle measurements, where raw FRs biochar shows a higher contact angle (88°), indicating greater hydrophobicity compared to acid/glycerol + AEO biochar (66.4°) (Fig. 9b).

In summary, the adsorption of PFOA onto biochar surfaces involves a combination of electrostatic interactions, hydrogen bonding, and hydrophobic interactions. Raw FRs biochar primarily relies on robust hydrophobic interactions facilitated by its extensive aromatic structures, while acid/glycerol + AEO biochar exhibits stronger electrostatic and hydrogen bonding due to its higher abundance of functional groups. These differences highlight the distinct adsorption mechanisms of each biochar, underscoring their potential for targeted environmental remediation applications, particularly in sequestering persistent organic pollutants like PFOA.

3.7. Minimum selling price and CO_2 emissions for adsorbent production

Before evaluating the MSP and CO_2 emissions of FRs-derived biochars, a mass balance analysis was conducted based on

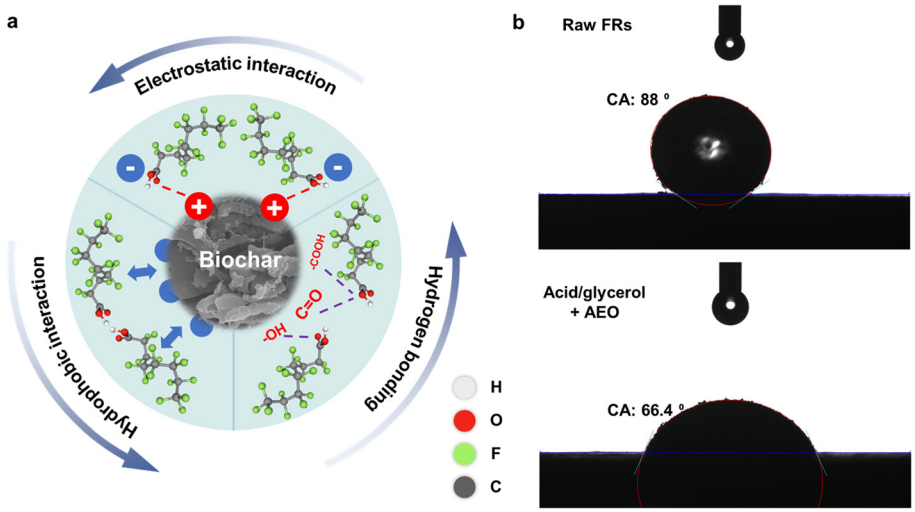

Fig. 9 Schematic representation the mechanisms of PFOA adsorption on biochar samples, highlighting electrostatic interactions, hydrogen bonding, and hydrophobic interactions (a). Contact angle measurements for raw FRs and acid/glycerol + AEO biochar samples (b).

1 kg of FRs in a cascading biorefinery process (Fig. 10). Initially, the FRs consisted of 476 g of lignin, 489 g of cellulose, 21 g of xylan, and 14 g of ash. After acid/glycerol + AEO pretreatment, the solid phase retained 469 g of lignin (98.5%) and 464 g of cellulose (94.9%), while the liquid phase comprised 7 g of lignin, 25 g of cellulose, 15 g of xylan, and 12 g of ash. Enzymatic hydrolysis then converted the cellulose into 425 g of glucose, equating to 91.6% of the cellulose. This glucose was fermented to produce 198.3 g of ethanol, representing 46.6% of the glucose. During the pyrolysis stage, 183.3 g of bio-oil was generated, with phenol constituting 143 g, or 77.5%, of the bio-oil. Additionally, 237.8 g of biochar was produced, representing 50.5% of the lignin. The biochar showed a PFOA adsorption capacity of 25.6 mg g^{-1}, underscoring its potential for environmental remediation.

The selection of effective pollutant removal methods hinges critically on the economic viability of the adsorbents employed in batch adsorption processes. Recognizing that cost considerations are paramount in decision-making, it is essential to incorporate the expenses associated with adsorbents when determining the optimal strategies for removing PFOA. In this context, our FRs-derived biochars emerge as a promising alternative. An economic analysis, adapted from a report by the NREL,[22] estimated the MSP of these biochars based on an annual production capacity of 183 ktons of biochar as the primary product, alongside 153 ktons of ethanol and 142 ktons of bio-oil derived from 772 ktons of FRs annually. This analysis was conducted based on data derived from mass balance calculations, ensuring a robust evaluation of input and output flows (Fig. 10). The comprehensive results of this evaluation are summarized in Table 4. The MSP of the FRs-derived biochar is estimated at US$ 41.81 per ton. Notably, the consumption of sulfuric acid and glycerol had the highest cost impact, contributing an additional US$ 30.72 per ton.

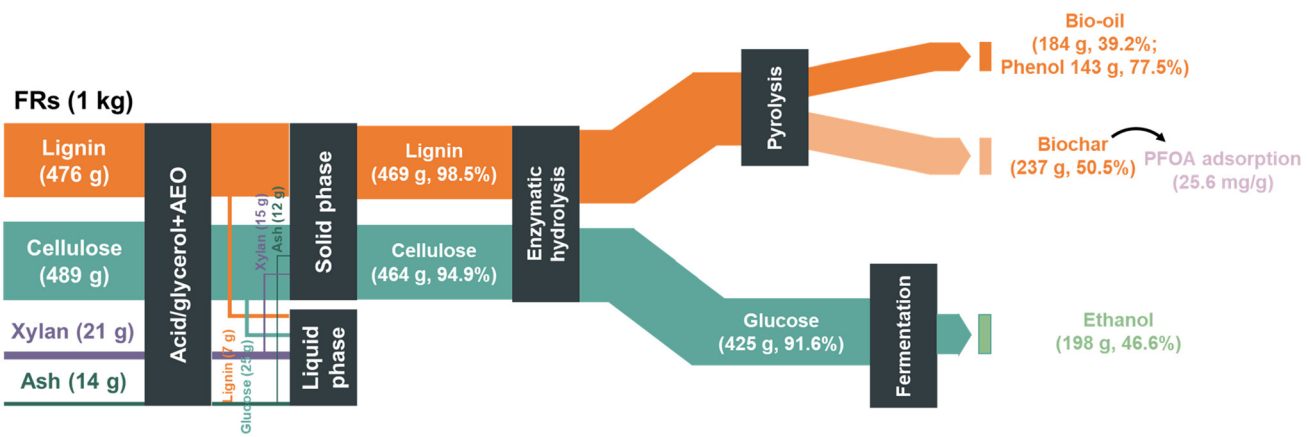

Fig. 10 Mass balance diagram of 1 kg FRs conversion in a cascading biorefinery, highlighting the production of ethanol, bio-oil, and PFOA-adsorbing biochar.

Table 4 Annual cost for production of biochar adsorbent (183 kton per yr) as the main product and ethanol (153 kton per yr) and bio-oil (142 kton per yr) as byproducts from FRs (773 kton per yr)

Stage	Annual cost ($kton per yr)	Cost per unit of product (US$ per ton adsorbent)
Feedstock collection, processing, storage, and transport	27 025 316[a]	14.75
Sulfuric acid	28 554 370[b]	15.59
Glycerol	27 734 952[c]	15.13
Ammonia	4 000 000	2.18
Glucose (enzyme production)	11 800 000	6.44
Other raw materials	7 900 000	4.31
Waste disposal	1,500,000	0.82
Plant electricity use	14 274 000	7.79
Fixed cost	10 700 000	5.84
Capital depreciation	13 400 000	7.31
Average income tax	7 500 000	4.09
The average return on investment	34 600 000	18.88
Biooil (byproduct)	−69 067 357[d]	−37.69
Ethanol (byproduct)	−113 585 044	−61.99
MSP (US$ per ton)		41.81[e]

[a] The cost was estimated at $35 per dry ton.[23] [b] Sulfuric acid usage was estimated at 219 649 tons per year, costing $130 per ton.[24] [c] Assuming 1% loss of the circulating glycerol, estimated at 8,279,090 tons per year, the cost is $335 per ton.[25] [d] Assuming bio-oil and ethanol selling prices of $486 and 741 per ton.[26] [e] MSP = 15.13 × Glycerol Loss (%) + 26.68.

Conversely, producing bio-oil and ethanol as byproducts provided a substantial cost offset, reducing the overall expense by US$ 99.68 per ton of adsorbent. Consequently, the cost of the adsorbent required to remove 1 gram of PFOA was estimated to range between 1.5 and 1.8 cents. For comparative context, Praveen *et al.*[47] conducted a techno-economic feasibility study on the use of biochar as a biosorbent for basic dye sequestration, reporting total production costs of US$ 51 to 54 per ton for biochar derived from the pyrolysis of coconut shells, groundnut shells, and rice husks. They estimated the adsorbent cost for removing 1 gram of dye to lie between 1.1 and 5.4 cents. Moreover, the literature reports a broad range of expenses for various biochar adsorbents, from US$ 52 to US$ 126 450 per ton,[48] thereby highlighting the competitive positioning of FR-derived biochars within this spectrum.

The environmental impact assessment, particularly CO_2 emissions, reinforces the sustainability profile of FR-derived biochar. Estimated emissions for its production are 936 grams of CO_2 per kilogram of adsorbent (Fig. 11). This calculation assumes that lignin, instead of being used for onsite energy generation, is directed to pyrolysis for adsorbent production, with electricity and heat sourced externally. In comparison, life cycle assessments of activated carbon, a widely used alternative for PFOA adsorption,[49] report CO_2 emissions ranging from 10 to 18 300 grams per kilogram, depending on methodology and system boundaries.[50] These findings suggest a lower carbon footprint for FRs-derived biochars, which provide a sustainable alternative and reduce reliance on energy-intensive activated carbon.

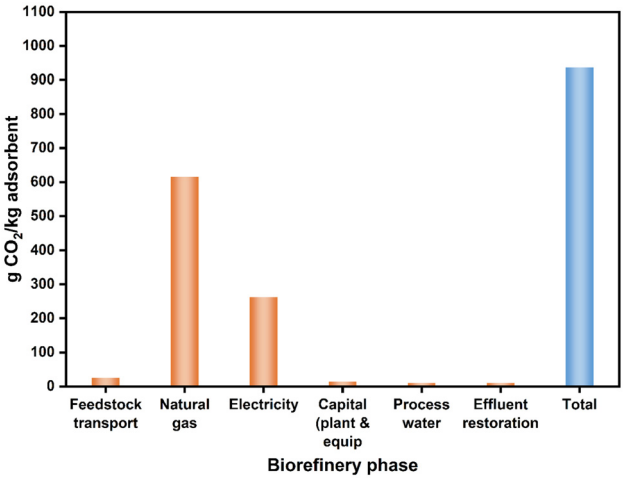

Fig. 11 CO_2 emissions across different categories in the biorefinery process for adsorbent production using the EBAMM.[27]

Overall, FRs-derived biochars offer a compelling combination of economic and environmental advantages. Integrating byproduct recovery within a biorefinery framework supports a more circular bioeconomy and enhances the financial feasibility of biochar production for environmental remediation applications. This approach aligns with sustainable development goals, providing a viable pathway for cost-effective and environmentally responsible pollutant removal technologies.

4. Conclusions

This study highlights the potential of a cascading biorefinery approach to convert FRs into high-value products such as ethanol, bio-oil rich in phenols, and biochar. By integrating advanced acid/glycerol pretreatment with AEO surfactants, we achieved efficient fractionation and conversion of FRs, resulting in significant yields of ethanol and bio-oil. The pyrolysis process further demonstrated the utility of biochar in environmental remediation, particularly in adsorbing PFOA at minimal cost, thus offering a sustainable solution for pollution control. Economic analysis supports the viability of this model, with competitive biochar pricing and reduced CO_2 emissions, aligning with sustainability goals. This research underscores the potential of FRs as a renewable feedstock, advancing the circular bioeconomy and reducing dependence on fossil fuels.

Future research should incorporate comprehensive life cycle assessment (LCA) and techno-economic analysis (TEA) to evaluate the sustainability and economic feasibility of the cascading biorefinery approach. These analyses will provide insights into environmental impacts, operational costs, and market dynamics while exploring integration with existing

biomass supply chains and engaging with policymakers to enhance scalability and reinforce the role of FRs as a renewable feedstock in sustainable biofuel production.

Author contributions

Yuting Tan: methodology, formal analysis, software. Meysam Madadi: supervision, conceptualization, visualization, writing – review & editing. Guojie Song: software, methodology. Chihe Sun: validation, data curation. Mahdy Elsayed: methodology, formal analysis. Fubao Sun: supervision, validation, writing – review & editing. Vijai Kumar Gupta: validation, writing – review & editing.

Data availability

The data supporting this article have been included as part of the ESI.†

Conflicts of interest

There are no conflicts to declare.

Acknowledgements

This work was supported by the State Key R&D Program (2022YFC2104601) and the National Natural Science Foundation of China (52106245; 22278189; 22478154).

References

1 M. Elsayed, M. Eraky, A. I. Osman, J. Wang, M. Farghali, A. K. Rashwan, I. H. Yacoub, D. Hanelt and A. Abomohra, *Environ. Chem. Lett.*, 2024, **22**, 609–634.
2 N. R. Baral, C. Quiroz-Arita and T. H. Bradley, *Environ. Sci. Technol.*, 2018, **52**, 14528–14537.
3 C. Xu, E. Paone, D. Rodríguez-Padrón, R. Luque and F. Mauriello, *Chem. Soc. Rev.*, 2020, **49**, 4273–4306.
4 M. Chang, X. Wang, Q. Lin, R. Li, L. Zhao, J. Ren and F. Zhang, *Green Chem.*, 2022, **24**, 6232–6240.
5 A. Siddiqa, Z. Yhobu, D. H. Nagaraju, M. Padaki, S. Budagumpi, V. R. Pasupuleti and J.-W. Lim, *Energy Fuels*, 2023, **37**, 2498–2519.
6 Y. Sun, Z. Wang, Y. Liu, X. Meng, J. Qu, C. Liu and B. Qu, *Energies*, 2019, **13**, 21.
7 C. Sun, H. Ren, F. Sun, Y. Hu, Q. Liu, G. Song, A. Abdulkhani and P. L. Show, *Bioresour. Technol.*, 2022, **344**, 126264.
8 C. Sun, G. Song, Z. Pan, M. Tu, M. Kharaziha, X. Zhang, P.-L. Show and F. Sun, *Bioresour. Technol.*, 2023, **368**, 128356.
9 G. Song, L. Liu, M. Madadi, M. Elsayed, C. Sun, Q. Liu, J. Zhang, F. Sun and A. Ashori, *Energy Convers. Manage.*, 2024, **319**, 118896.
10 G. Song, C. Sun, Y. Hu, C. Wang, C. Xia, M. Tu, E. Zhang, P.-L. Show and F. Sun, *J. Phys.: Energy*, 2023, **5**, 014015.
11 D. V. Suriapparao, N. Pradeep and R. Vinu, *Energy Fuels*, 2015, **29**, 2571–2581.
12 X. Lu and X. Gu, *Biotechnol. Biofuels Bioprod.*, 2022, **15**, 106.
13 M. Elsayed, M. Madadi, G. Song, Z. Zhou, H. Wang, J. Wang, J. Zhang, M. Aghbashlo and M. Tabatabaei, *Fuel*, 2024, **376**, 132678.
14 G. Song, H. Zhang, M. Madadi, Z. Chen, H. Wang, A. Xia, A. Samimi, C. Sun, X. Meng and A. J. Ragauskas, *Green Chem.*, 2024, **26**, 10123–10138.
15 G. Song, M. Madadi, X. Meng, C. Sun, M. Aghbashlo, F. Sun, A. J. Ragauskas, M. Tabatabaei and A. Ashori, *Chem. Eng. J.*, 2024, **481**, 148713.
16 E. Lizundia, F. Luzi and D. Puglia, *Green Chem.*, 2022, **24**, 5429–5459.
17 Y. Yea, G. Kim, D. Wang, S. Kim, Y. Yoon, S. S. Elanchezhiyan and C. M. Park, *Chem. Eng. J.*, 2022, **430**, 132837.
18 G. Song, C. Sun, M. Madadi, S. Dou, J. Yan, H. Huan, M. Aghbashlo, M. Tabatabaei, F. Sun and A. Ashori, *Bioresour. Technol.*, 2024, **395**, 130358.
19 M. R. Mukasekuru, J. Hu, X. Zhao, F. F. Sun, K. Pascal, H. Ren and J. Zhang, *ACS Sustainable Chem. Eng.*, 2018, **6**, 12787–12796.
20 Z.-Z. Liu, C.-G. Pan, F.-J. Peng, J.-J. Hu, H.-M. Tan, R.-G. Zhu, C.-Y. Zhou, H. Liang and K. Yu, *Bioresour. Technol.*, 2024, **408**, 131157.
21 Y. Zhang, X. Tan, R. Lu, Y. Tang, H. Qie, Z. Huang, J. Zhao, J. Cui, W. Yang and A. Lin, *ACS ES&T Water*, 2023, **3**, 817–826.
22 D. Humbird, Process design and economics for biochemical conversion of lignocellulosic biomass to ethanol, **https://cir.nii.ac.jp/crid/1573668924089556992** (accessed October 13, 2024).
23 D. Humbird, R. Davis, L. Tao, C. Kinchin, D. Hsu, A. Aden, P. Schoen, J. Lukas, B. Olthof and M. Worley, *Process design and economics for biochemical conversion of lignocellulosic biomass to ethanol: dilute-acid pretreatment and enzymatic hydrolysis of corn stover*, National Renewable Energy Lab. (NREL), Golden, CO (United States), 2011.
24 Sulfuric acid China Domestic Price, **https://www.echemi.com/pcp/sulfuric-acid-pid_Rock19440.html**, (accessed October 14, 2024).
25 Glycerine Price Trend and Forecast, **https://www.chemanalyst.com/Pricing-data/glycerine-1168**, (accessed October 14, 2024).
26 Ethanol Price Trend and Forecast, **https://www.chemanalyst.com/Pricing-data/ethanol-13**, (accessed October 14, 2024).
27 A. E. Farrell, R. J. Plevin, B. T. Turner, A. D. Jones, M. O'Hare and D. M. Kammen, *Science*, 2006, **311**, 506–508.

28 Y. Xing, L. Bu, D. Sun, Z. Liu, S. Liu and J. Jiang, *Fuel*, 2016, **177**, 142–147.
29 M. Madadi, G. Song, V. K. Gupta, M. Aghbashloh, C. Sun, F. Sun and M. Tabatabaei, *Green Chem.*, 2023, **25**, 7141–7156.
30 K. Holmberg, *Colloids Surf., B*, 2018, **168**, 169–177.
31 M. Madadi, M. Elsayed, G. Song, R. Kumar, M. Mahmoud-Aly, B. Basak, B.-H. Jeon and F. Sun, *Chem. Eng. J.*, 2023, **465**, 142881.
32 S. D. Shinde, X. Meng, R. Kumar and A. J. Ragauskas, *Green Chem.*, 2018, **20**, 2192–2205.
33 C. Zhang, Q. Xue, J. Hou, A. Mohsin, M. Zhang, M. Guo, Y. Zhu, J. Bao, J. Wang and W. Xiao, *J. Agric. Food Chem.*, 2019, **67**, 12002–12012.
34 M. Xiong, J. Huang, X. He, Z. Zhou, X. Qu, S. Faisal and A. Abomohra, *Fuel*, 2023, **331**, 125710.
35 H. Nikkhah, A. Tavasoli and S. Jafarian, *Energy Convers. Manage.*, 2020, **225**, 113392.
36 R. P. Lopes and D. Astruc, *Coord. Chem. Rev.*, 2021, **426**, 213585.
37 D. Cai, J. Wen, Y. Wu, C. Su, H. Bi, Y. Wang, Y. Jiang, P. Qin, T. Tan and C. Zhang, *Bioresour. Technol.*, 2024, **394**, 130231.
38 H. Chen, J.-J. Wang, P.-J. Ku, M. T.-K. Tsui, R. B. Abney, A. A. Berhe, Q. Zhang, S. D. Burton, R. A. Dahlgren and A. T. Chow, *Environ. Sci. Technol.*, 2022, **56**, 12678–12687.
39 H. Machado, A. F. Cristino, S. Orišková and R. Galhano dos Santos, *Reactions*, 2022, **3**, 118–137.
40 P. Tyagi, S. Agate, O. D. Velev, L. Lucia and L. Pal, *Environ. Sci. Technol.*, 2022, **56**, 2071–2095.
41 M. Varsha, P. S. Kumar and B. S. Rathi, *Chemosphere*, 2022, **287**, 132270.
42 M. Belluati, S. Tabasso, E. C. Gaudino, G. Cravotto and M. Manzoli, *Green Chem.*, 2024, **26**, 8642–8668.
43 S. Kundu, S. Patel, P. Halder, T. Patel, M. H. Marzbali, B. K. Pramanik, J. Paz-Ferreiro, C. C. de Figueiredo, D. Bergmann and A. Surapaneni, *Environ. Sci.: Water Res. Technol.*, 2021, **7**, 638–649.
44 W. Tang, B. L. G. L. Zanli and J. Chen, *Bioresour. Technol.*, 2021, **341**, 125794.
45 W. Jiang, Y. Cai, D. Liu, X. Yu and Q. Wang, *Environ. Res.*, 2024, **241**, 117662.
46 J. Kim, L. Chernysheva, J. Xu, M. McClure, D. R. Latulippe, W. A. Phillip and K. Doudrick, *ACS ES&T Eng.*, 2024, **4**, 995–1006.
47 S. Praveen, R. Gokulan, T. B. Pushpa and J. Jegan, *J. Indian Chem. Soc.*, 2021, **98**, 100107.
48 A. S. El-Shafie, E. Rahman, Y. GadelHak, R. Mahmoud and M. El-Azazy, *Spectrochim. Acta, Part A*, 2024, **306**, 123621.
49 J. Xu, Z. Liu, D. Zhao, N. Gao and X. Fu, *Sci. Total Environ.*, 2020, **723**, 137757.
50 A. Vilén, P. Laurell and R. Vahala, *J. Environ. Manage.*, 2022, **324**, 116356.
51 Y. Lu, H. Wang, Y.-Y. Lu, Z.-Q. Ren, N. Gao, J.-J. Wang, B.-C. Huang and R.-C. Jin, *J. Environ. Manage.*, 2025, **373**, 123607.
52 X.-M. Chen, H.-Y. Li, C.-C. Wei, J. Cheng, J. Diao, B. Xie and F. Pan, *ACS Sustain. Chem. Eng.*, 2025, **13**(3), 1327–1335.
53 X.-R. Pan, P.-K. Shang-Guan, S.-H. Li, C.-H. Zhang, J.-M. Lou, L. Guo, L. Liu and Y. Lu, *Environ. Res.*, 2025, **267**, 120645.
54 L. Fu, J. Wang, X. Fu and G. Zhao, *Int. J. Hydrogen Energy*, 2025, **98**, 1034–1043.
55 L. Sun, Z. Jiang, B. Yuan, S. Zhi, Y. Zhang, J. Li and A. Wu, *Chem. Eng. Res. Des.*, 2021, **174**, 71–78.